ACS APPLIED MATERIALS & INTERFACES

Research Article

www.acsami.org

Concerted Mitigation of O···H and C(π)···H Interactions Prospects Sixfold Gain in Optical Nonlinearity of Ionic Stilbazolium Derivatives

Jacqueline M. Cole,*[,†,¶,‡] Tze-Chia Lin,*[,†,‡] Alison J. Edwards,[§] Ross O. Piltz,[§] Griet Depotter,[⊥] Koen Clays,[⊥] Seung-Chul Lee,[#] and O-Pil Kwon[#]

[†]Cavendish Laboratory, University of Cambridge, J. J. Thomson Avenue, Cambridge, CB3 0HE, U.K.

[¶]Argonne National Laboratory, 9700 S. Cass Avenue, Argonne, Illinois 60439, United States

[§]Bragg Institute, Australian Nuclear Science and Technology Organization, New Illawarra Road, Lucas Heights, NSW 2234, Australia

[⊥]Department of Chemistry, University of Leuven, Celestijnenlaan 200D, 3001 Leuven, Belgium

[#]Department of Molecular Science and Technology, Ajou University, Suwon 443-749, S. Korea

Supporting Information

ABSTRACT: DAST (4-dimethylamino-*N*-methyl-4-stilbazolium tosylate) is the most commercially successful organic nonlinear optical (NLO) material for frequency-doubling, integrated optics, and THz wave applications. Its success is predicated on its high optical nonlinearity with concurrent sufficient thermal stability. Many chemical derivatives of DAST have therefore been developed to optimize their properties; yet, to date, none have surpassed the overall superiority of DAST for NLO photonic applications. This is perhaps because DAST is an ionic salt wherein its NLO-active cation is influenced by multiple types of subtle intermolecular forces that are hard to quantify, thus, making difficult the molecular engineering of better functioning DAST derivatives. Here, we establish a model parameter, η_{inter}, that isolates the influence of intermolecular interactions on second-order optical nonlinearity in DAST and its derivatives, using second-harmonic generation (SHG) as a qualifier; by systematically mapping intercorrelations of all possible pairs of intermolecular interactions to η_{inter}, we uncover a relationship between concerted intermolecular interactions and SHG output. This correlation reveals that a sixfold gain in the intrinsic second-order NLO performance of DAST is possible, by eliminating the identified interactions. This prediction offers the first opportunity to systematically design next-generation DAST-based photonic device nanotechnology to realize such a prospect.

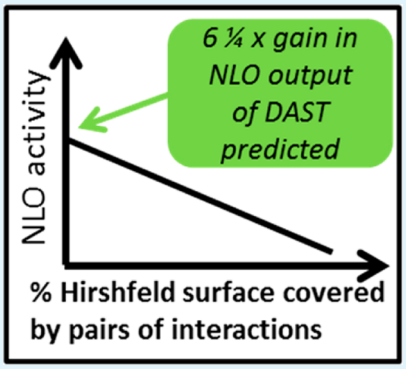

KEYWORDS: *organic nonlinear optics, DAST, intermolecular interactions, molecular engineering*

INTRODUCTION

A focus on discovering NLO performance improvements in derivatives of DAST (4-dimethylamino-*N*-methyl-4-stilbazolium tosylate; Figure 1) is considered to be important[1−3] since DAST is the most commercially successful organic NLO material.[4] Moreover, DAST is one of few organic compounds that offer adequate thermal stability for practical NLO applications; and yet, organic compounds are becoming increasingly desirable for optoelectronic device technology in light of environmental considerations and the increasing need for the very fast optical response times that only organics can afford.[5] It is electronic charge transfer that enables this fast NLO response in organic molecules, in contrast to the much slower ionic displacement that drives NLO mechanisms in their inorganic counterparts. Accordingly, one can relate the electronic structure of an organic material to its NLO properties.[6] The first hyperpolarizability, β, is the molecular measure of second-order optical nonlinearity, which may manifest as SHG; it relates to charge transfer in an electronic structure via its linear proportionality to the electronic polarizability of a molecule, when subjected to an electric field.

Curiously, the dispersion-free (static) hyperpolarizability of the isolated DAST cation (β_0 = 120 × 10^{-30} esu)[7] determined

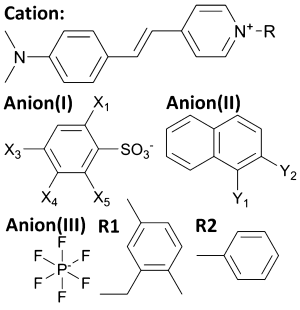

#	Name	R	Anion:X/Y
[1]	DAST	CH_3	(I):X_3=CH_3,$X_{1,4\&5}$=H
[2]	DSTMS	CH_3	(I):$X_{1,3\&5}$=CH_3,X_4=H
[3]	DSPFS	CH_3	(I):X_3=CF_3,$X_{1,4\&5}$=H
[4]	DSMOS	CH_3	(I):X_3=OCH_3,$X_{1,4\&5}$=H
[5]	DSDMS	CH_3	(I):$X_{3\&5}$=CH_3,$X_{1\&4}$=H
[6]	DSNS-1	CH_3	(II):Y_1=SO_3^-,Y_2=H
[7]	DAPSH	R2	(III)
[8]	BP3	R1	(I):X_3=CH_3,$X_{1,4\&5}$=H

Figure 1. Schematic chemical diagrams of DAST [**1**] and seven closely related derivatives [**2**]−[**8**].

Received: November 24, 2014
Accepted: February 5, 2015
Published: February 5, 2015

ACS Publications © 2015 American Chemical Society

DOI: 10.1021/am508213c
ACS Appl. Mater. Interfaces 2015, 7, 4693−4698

Table 1. Summary of the Structural and SHG Properties for [1]−[8]

	compound ID[a]							
	[1] DAST	[2] DSTMS	[3] DSPFS	[4] DSMOS	[5] DSDMS	[6] DSNS-1	[7] DAPSH	[8] BP3
Part I: Structural and NLO Properties								
references	this work and ref 1	ref 2	ref 18	ref 17	ref 2	ref 2	ref 16	this work and ref 15
space group	*Cc*	*Cc*	*Cc*	*P*1	*P*1	*P*1	*Cc*	$P2_1$
N (10^{-27} m^{-3})	1.906	1.769	1.850	1.904	1.843	1.789	2.033	1.480
θ (deg)[b]	20	23	20	1.8	0	0	15.5	79
β_0^{zzz} (10^{-30} esu)[c]	120	120	120	120	120	120	125	180
η_{exp}[d]	1.00	1.00	0.90	0.90	0.70	0.70	0.85	0.54
η_{inter}	1.00	1.11	0.98	0.84	0.76	0.79	0.83	1.98
Part II: All Short Contacts between the Core Cations and Neighboring Anions, Å[e]								
H(2)...π/O[f]	2.846	2.802	2.860	2.744	2.679	2.661		2.255
H(3)...O	2.244	2.416	2.474	2.306	2.317	2.279		(2.905)
H(8)...O	2.211	2.340	2.337	2.276	2.398	2.443		2.419
H(10)...O	(2.980)	(3.046)	(3.040)	(2.962)	(3.108)	(3.275)		(2.728)
H(11)...O/π[f]	(2.657)	(3.130)	(2.918)	(2.685)	(2.648)	2.611		
H(13)...π	2.927	(3.031)	(3.194)	2.840	2.809	2.912		(3.176)
H(14)...O	(3.185)	(2.750)	(2.922)	(3.523)	(3.218)	2.523		2.530
H(7)...O	2.290	2.301	2.301	(2.723)	(2.775)	2.254		2.216
H(5)...O	(2.658)	(2.774)	(2.656)	(2.608)	(2.729)	(2.954)		(2.822)
H(6)...O	2.201	2.418	2.335	2.255	2.451	2.392		2.478
H($1_{A/B}$)...O	2.247	2.339	2.333	2.557	2.167	(2.669)		2.214
H($15_{A/B/C}$)...O	2.436	2.500	2.434	(2.926)	2.577	2.439		(3.373)
H($16_{A/B/C}$)... π/O[f]	2.761	2.927	2.957	2.866	2.929	2.775		(2.902)
Part III: Fractions of the Hirshfeld Surface Area Coverage, %								
C...H/C/N[g]	19.6	19.0	18.8	19.4	19.1	19.0	22.1	18.6
H...H/N/F[h]	48.1	51.8	48.9	47.1	50.5	45.8	41.4	57.1
N...C/H/N[i]	2.0	1.6	1.7	2.0	1.8	1.7	1.3	1.1
H...C(π) cation to anion[j,l]	18.5	17.6	18.6	18.6	18.0	22.8	10.4	0
H...O/F[k,l]	12.0	10.0	11.9	13.1	10.8	10.7	24.8	10.7

[a]Part I: Compounds listed were searched/selected from the Cambridge Structural Database (CSD) and the criteria of acceptance were as follows: organic compounds where the accurate crystallographic data (R < 7.5%) and the powder SHG data were both available (see Supporting Information for full details on selection criteria). [b]Part I: Owing to the one-dimension charge-transfer nature of the DAST derivatives, only the angle between the molecular charge-transfer direction and the polar crystal axis affects the overall macroscopic SHG efficiency. [c]Part I: For [**1**] and [**7**], the averaged β_0 from the literature (see ref 7, measured by the hyper-Rayleigh scattering (HRS) method) were given; for [**2**]−[**6**], the same β_0 as compound [**1**] was assumed since they all share the same cation; for [**8**], β_0 was measured by HRS (see Experimental Methods). [d]Part I: Data acquired from the literature.[9−14] (See refs 1, 2, 18, 17, 16, and 15 for [**1**], [**2**, **5**, **6**], [**3**], [**4**], [**7**], and [**8**], respectively.) [e]Part II: Criteria of acceptance as short contacts: d(H...O) < 2.6 Å, d(H...π) < 3.0 Å. The number in the brackets indicates that the contact distance is longer than the above criteria and is only given here for completeness. For the cases where the hydrogen donors interact with multiple acceptors, only the strongest (shortest) contact was listed. Compound [**4**] contains four pairs of cations and anions in the asymmetric unit, and therefore, the contact distances listed here are the averaged values from the four cations. [f]Part II: For H(2), H(11), and H(16A/B/C), the hydrogen atoms may interact with two types of acceptors; the distances were underlined if they are associated with the second acceptor. [g]Part III: The sum of the percentages from C...H (major), C...C (minor, ~5%), and C...N (minor, <2%) contacts. [h]Part III: The sum of the percentages from H...H (major), H...N (minor, <1%), and H...F (only existence in [**5**], 10.7%) contacts. [i]Part III: The sum of the percentages from N...C, N...H, and N...N contacts. [j]Part III: For [**1**]−[**7**], the majority of H...C(π) contacts interactions here are cation-to-anion in nature which involve the principal conjugating atoms (or fragments). The total calculated H...C contact-surface coverage for [**8**] is 12.6%; however, this value is indiscriminate on ion...ion pairing types; classifying them separately reveals that these H...C interactions are essentially associated with weak cation-to-cation H...C contacts involving atoms that do not lie in the main charge-transfer path; cation-to-anion contributions are null. [k]Part III: The contact area percentages of the H...O (or H...F) hydrogen bonds for [**1**]−[**6**] and [**8**] (or [**7**]). Associated fingerprint plots of [**1**] and [**8**] are provided in Figure S5 of the Supporting Information.

by hyper-Rayleigh scattering (see Table S1 in the Supporting Information) is over 3 times larger than that of its ionic compound evaluated within a crystalline environment via Maker-Fringe experiments [β_{zzz}^{cry} = (37 ± 10) × 10^{-30} esu].[8] Several crystallographic factors may be responsible for this difference, as judged by the oriented-gas model that relates β_{zzz}^{cry} to the macroscopic SHG output **d** (eq 1).[9]

$$d_{ijk} = \frac{1}{2}\chi_{ijk} = \frac{1}{2}\frac{N}{n(g)}F_{ijk}\sum_{s}^{n(g)}\sum_{lmn}^{3}\cos\theta_{il}^{s}\cos\theta_{jm}^{s}\cos\theta_{kn}^{s}\beta_{lmn}^{cry} \quad (1)$$

where $\chi_{ijk}(d_{ijk})$ are the macroscopic second-order NLO susceptibilities (coefficients); N, $n(g)$, and F_{ijk} are the molecular number density, equivalent positions (index by s) per unit cell, and local-field correction factor, respectively; θ_{im}^{s} are the angles between the Cartesian and molecular axes.

Indeed, crystal engineering attempts to improve SHG in DAST derivatives have exploited the relationship between θ and d.[1] However, no model that specifically relates intermolecular interactions to $\boldsymbol{\beta}$ *exclusively* has yet been proposed, despite their evident control over SHG performance in many organic NLO materials. Such studies on organic materials have identified intermolecular interactions that

DOI: 10.1021/am508213c
ACS Appl. Mater. Interfaces 2015, 7, 4693−4698

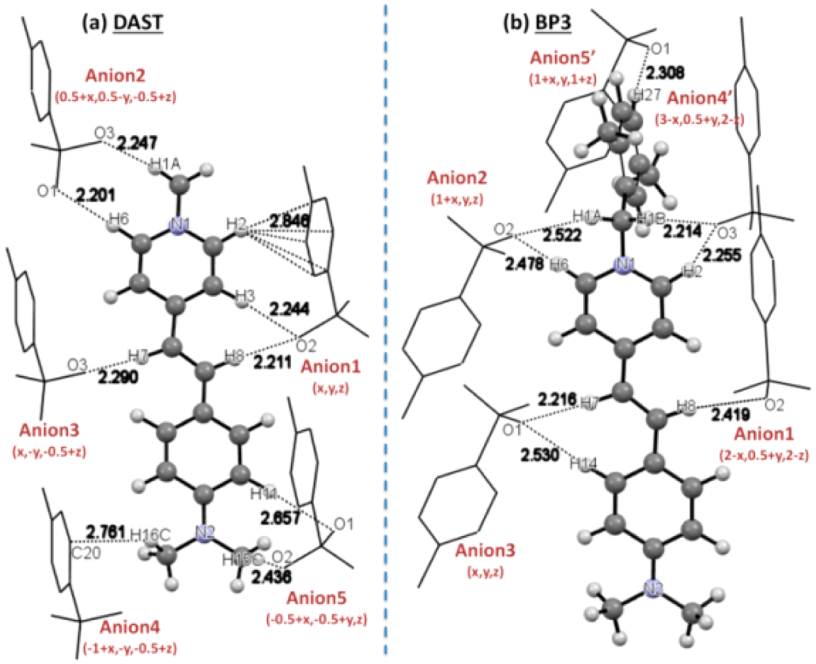

Figure 2. Cation−anion interactions of DAST [**1**] and [**8**]. The hydrogen atoms of the anions are omitted for clarity.

visually align well with the molecular charge-transfer axes of the NLO material and so will augment $\boldsymbol{\beta}$.[10−14] Yet, intermolecular interactions that decrease $\boldsymbol{\beta}$, as likely in DAST, given $\beta_0 \gg \beta_{zzz}^{cry}$, are much more subtle to discern.

Since $\beta_0 \gg \beta_{zzz}^{cry}$ for DAST, we postulated that a sizable improvement of the macroscopic SHG response of DAST derivatives may be achievable, if specific intermolecular interactions, that are deleterious to $\boldsymbol{\beta}$, can be identified; thus, advocating a refocusing on crystal engineering efforts toward their removal.

To this end, we devised a new model parameter, η_{inter}, which expresses contributions to $\boldsymbol{\beta}$ exclusively from intermolecular interactions, and then deduced a correlation between $\boldsymbol{\beta}$ and specific intermolecular interactions. Neutron diffraction was employed to probe key interactions accurately. Finally, we use this correlation to forecast how much NLO gain in DAST derivatives is possible. Given DAST leads the organic NLO industry, this prediction attests high promise for sustaining its commercial market.

RESULTS AND DISCUSSION

The new model parameter, $\eta_{inter} = ((\eta_{exp})/(\eta_{calc}))^{1/2} = ((d_{exp}{}^2/d_{exp\ DAST}{}^2)/(d_{calc}{}^2/d_{calc\ DAST}{}^2))^{1/2}$. η_{exp} is the orientationally averaged macroscopic SHG output d^2 of a DAST derivative obtained from powder SHG experiments,[1,15−17] normalized to that of DAST; reducing **d** to a one-dimensional problem is appropriate for DAST since it is dominated by one component (d_{111}).[8] η_{calc} refers to the derivation of $\langle d^2 \rangle$ from the oriented-gas model (eq 1), also relative to DAST, employing values of N and θ taken from crystallographic data of each compound; and yet, β_0 is from hyper-Rayleigh scattering measurements of each cation, so one assumes $\beta_{zzz}^{cry} = \beta_0$ and $F = 1$, i.e., assume that intermolecular interactions dominate the local-field factors. Forming the ratio, η_{inter}, cancels out N, θ, and β_0 effects, rendering η_{inter} as the difference in SHG efficiency arising *exclusively* from the influence of the crystal field forces relative to those of DAST. Naturally, $\eta_{inter} = 1$ for DAST. Since $\sqrt{\langle d^2 \rangle} \propto \boldsymbol{\beta}$, those compounds with η_{inter} smaller (or larger) than unity indicate that their crystal field forces compromise their SHG activity more (or less) than the 3.25-fold reduction seen in DAST ($\beta_0/\beta_{zzz}^{cry}$), caused by such forces.

For DAST ([**1**]) and seven closely related derivatives ([**2**]−[**8**]), η_{inter} was enumerated using β_0 values and crystal data (for N and θ) from the literature[1,16−18] ([**1**]−[**7**]) or in-house hyper-Rayleigh scattering[19] ([**8**]) and neutron diffraction experiments ([**1**], [**8**]; see Experimental Methods and Table 1). A correlation was initially sought between η_{inter} and each type of nonbonded short contact in [**1**]−[**8**], as listed in Table 1 and displayed in Figure 2 for [**1**] and [**8**]. This tentatively suggested a weak linear relationship between η_{inter} and the H(2)...C(π) interaction length (correlation coefficient R^2 = 0.64, Figure S1 in the Supporting Information); c.f. cation...anion1 nonbonded contacts in Figures 2 and S2.

When considering correlations between η_{inter} and all possible pairs of intermolecular interactions, however, a striking correlation was discovered. Figure 3 shows a near-perfect linear correlation (R^2 = 0.91) between η_{inter} and the combined 3-D Hirshfeld surface area coverage (%)[20] of H...O and H...C(π) intermolecular interactions of [**1**]−[**8**].

Encouragingly, this strong correlation is reproducible using independent, albeit much more limited, SHG data (R^2 = 0.96), obtained from Maker-Fringe experiments on [**1**], [**2**], and [**7**] (Figure S4). The Hirshfeld surface concept[21] was employed here since this reflects the electron distribution differences between the isolated DAST cation (promolecule) and that in its crystalline environment (procrystal), i.e., precisely the intermolecular interactions that would differentiate β_0 and β_{zzz}^{cry}, per the central notion behind the definition of our model parameter η_{inter}.

This strong correlation reveals that *concerted* H...O and H...C(π) intermolecular interactions dominate the crystal field forces which impact SHG activity in DAST derivatives. The correlation manifests over a modest range, except for the case of [**8**] which stands out markedly, possessing, by far, the largest

DOI: 10.1021/am508213c
ACS Appl. Mater. Interfaces 2015, 7, 4693−4698

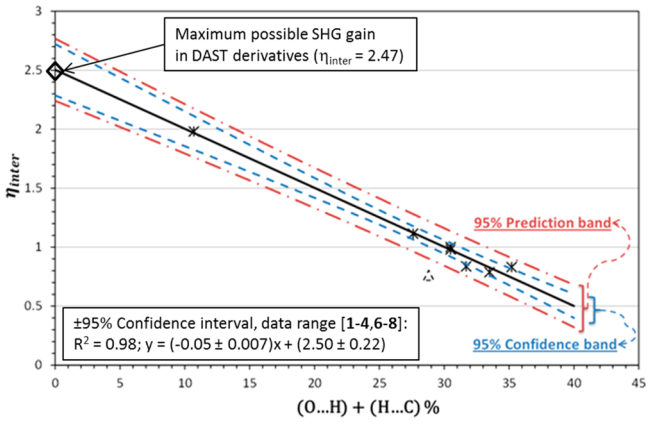

Figure 3. Linear correlations between η_{inter} and the total percentage of the Hirshfeld surface area coverage of H...O and H...C(π) contacts for [**1**]−[**4**] and [**6**]−[**8**]. It is helpful to note here that significant error is associated with the bottom-most data point that is associated with [**5**], so it is included in this figure for the sake of completeness, but was excluded in the regression analysis (see Figure S3 for more details). Correlation analysis between η_{inter} and (O...H) + (H...C) % afforded the 95% confidence band displayed between the two blue-dashed lines, with best-fit linear-correlation parameters given in the figure inset (bottom left). The associated 95% prediction band, bounded by the two red-dashed lines, offers an estimation range for the future data points based on our present analysis. The standard error of η_{inter} is ∼0.06, which is around 3−8% of all quoted powder SHG results used in this work. Checks were also made against possible artifacts, owing to the high statistical leverage of the top leftmost data point associated with [**8**]; a least-squares fit without [**8**] predicts η_{inter} = 2.28 in the zero limit and R^2 = 0.81, thus demonstrating good reliability of [**8**] within the observed trend.

$\eta_{inter} \approx 2$. Incidentally, it also exhibits the largest β_0 and β_{zzz}^{cry} values of all compounds in this set.

Neutron diffraction probed these intermolecular interactions in [**1**] and [**8**], to determine why this specific pair of hydrogen-bond types exclusively affords SHG enhancement in [**8**], yet generally diminishes SHG in DAST derivatives. Both [**1**] and [**8**] exhibit H...O interactions, the strongest (shortest) being bifurcated cation...anion hydrogen bonds associated with anion1 and anion4′ for [**1**] and [**8**], respectively (Figure 2). H...C(π) interactions in [**1**] and [**8**] differ markedly: again, the cation of [**1**] exhibits its closest interaction with anion1, while [**8**] lacks H...C(π) cation...anion interactions entirely (see Supporting Information, C′ in Figure S5); instead, it features only weak H...C(π) cation...cation interactions. This suggests that concerted H...O and H...C(π) cation...anion1 interactions dominate NLO effects in [**1**], while only H...O cation...anion4′ interactions control [**8**].

These concerted, attractive cation...anion interactions in [**1**] lie sideways to the intramolecular charge-transfer axis, which essentially runs between N1 and N2. Thus, supramolecular charge-transfer propagation is hindered, which deters macroscopic SHG output. In contrast, the R1 substituent in [**8**] (Figure 1) serves to induce a crystal packing arrangement, whose most attractive cation...anion interactions lie at a primary ICT terminus (N1) in the cation, while cation...cation forces are much weaker. As such, these cation..anion interactions are far less detrimental to charge propagation, and thus least affect macroscopic NLO activity. It is helpful to note that the rationalization of these SHG-governing interactions would not have been evident without first identifying the correlation in Figure 3.

An even more striking feature of this correlation is its predictive quality: by extrapolation to the limit, (O...H) + (H...C) % → 0, a DAST derivative removed of such interactions will afford η_{inter} = 2.5; i.e., this pair of interactions accounts for the majority (77%) of the 3.25-fold discrepancy between β_0 and β_{zzz}^{cry}. Given $\langle d^2 \rangle \propto \boldsymbol{\beta}^2$, η_{inter} = 2.5 translates macroscopically to d^2 becoming 6.25 times that of DAST when void of this pair of interactions. Again, analogous calculations from the Maker-Fringe SHG data are corroboratory (Figure S4 of the Supporting Information). This evidences that major improvements in the NLO performance of DAST are attainable, if crystal engineering efforts are suitably refocused to reach this limit.

CONCLUSIONS

This work therefore demonstrates that DAST can sustain its lead in the organic NLO commercial market by developing material derivatives with 6.25-fold gain in SHG performance. The predicted gain is based on our discovery of a strong linear correlation between the coupled Hirshfeld surface area coverage (%) of H...O and H...C(π) intermolecular interactions and the model parameter η_{inter}, which we devised to exclusively relate $\boldsymbol{\beta}$ to intermolecular interactions. This nontraditional, pairwise, assessment of intermolecular interactions was needed for identifying the most influential ones. It is encouraging to add that our experimental finding of deleterious effects of intermolecular interactions on SHG activity in DAST derivatives corroborates recent first-principles calculations; there, $\boldsymbol{\beta}$ was theoretically related to $\boldsymbol{\chi}^2$, by specifically incorporating polarization of surrounding ions into the DAST model.[22,23] More generally, this derivation stands to open up an area of analysis that specifically targets the structural needs of $\boldsymbol{\beta}$ at the supramolecular, and hence nanoscopic, level. This is important given the increasing attention toward NLO device applications for nanotechnology.[24,25]

EXPERIMENTAL METHODS

Hyper-Rayleigh Scattering. A methanol solution of [**8**] was subjected to incident light radiation of 800 nm, from a mode-locked femtosecond Ti:sapphire laser (Tsunami, Spectra Physics), which is pumped by a diode laser (Millennia, Spectra Physics), at a repetition frequency of 80 MHz with an average power of ∼2.1 W. The scattered second-harmonic light was collected via a condenser lens system, positioned at 90° scattering geometry in the $X-Y$ plane, and focused into a photomultiplier tube. To select the second-harmonic light, an appropriate interference filter was used. The results were derived from sample measurements at five successively diluted concentration fractions, $a/5$ (a = 1, 2, 3, 4, 5) of [**8**] with a parent concentration of 9.56 × 10^{-5} M. The sample was analyzed against Crystal Violet [$\beta_{xxx,800}$ = (338 ± 60) × 10^{-30} esu in methanol], a standard reference compound in this wavelength range, with a parent concentration of 8.58 × 10^{-4} M.[26] Differences in geometrical factor, due to octupolar reference and dipolar [**8**], were taken into account. Dilute solutions were used to ensure a linear dependence of $I_{2\omega}/I_{\omega}$ on concentration, precluding the need for Beer−Lambert correction factors. The high-frequency demodulation technique confirmed that there was no multiphoton fluorescence in [**8**] at the second-harmonic wavelength of 400 nm. Accordingly, the fluorescence-free hyperpolarizability value could be derived as the average value of the four modulation frequencies (80, 160, 240, and 320 MHz), yielding a $\boldsymbol{\beta}_{zzz}$ value of (580 ± 50) × 10^{-30} esu at 800 nm. The corresponding static hyperpolarizability β_0 was derived using a two-level model,[27−29] affording a value of (180 ± 20) × 10^{-30} esu.

DOI: 10.1021/am508213c
ACS Appl. Mater. Interfaces 2015, 7, 4693−4698

Neutron Diffraction. A (0.7 × 0.8 × 0.9) mm^3 [**1**] or (0.95 × 1.15 × 1.25) mm^3 [**8**] crystal, wrapped in thin aluminum foil and glued to an aluminum pin, was mounted onto the φ axis of the KOALA Laue diffractometer at the Bragg Institute, ANSTO, Australia.[30] Each sample was cooled to the experimental operational temperature (T = 120 K), using a helium closed-cycle refrigerator, and 19 Laue images were acquired per sample, each image being separated by 17° rotational increments in φ (perpendicular to the neutron beam) and using a neutron beam exposure time of 21 000 ([**1**]) or 7000 ([**8**]) s. Integrated intensities were corrected for detector efficiency, wavelength-dependent incident intensity normalization, secondary extinction, and time-dependent effects using the LaueG program suite.[31] Data with a $(\sin\theta/\lambda)_{max}$ = 0.63 Å cutoff were retained. This yielded a total of 1625 ([**1**]) or 1952 ([**8**]) symmetry-independent reflections against which a structural model was refined via full-matrix least-squares procedures using SHELXL-97.[32] The final structural models, with R1 ($I > 2\sigma(I)$) of 0.0495 ([**1**]) or 0.0352 ([**8**]), comprised refined positional and ADPs for all atoms, following the location of all hydrogen atoms directly from Fourier difference maps (see Supporting Information for further details).

Hirshfeld Surface Analysis. Crystal Explorer 3.0 was employed to enumerate the respective contributions of each intermolecular interaction to the Hirsheld surface area of an ion,[20] i.e., the isosurface that contains the region of space surrounding the subject ion in a crystal structure, where the electron distribution of the promolecule exceeds that due to any neighboring ion, subject to Hirshfeld atomic partitioning. Corresponding Fingerprint plots were generated from these Hirshfeld surfaces (Figure S5[21]). These plots represent two-dimensional mappings of the fraction of points on the surface as a function of the closest distances from the point to nuclei inside (d_i) and outside (d_e) this surface. By comparing the patterns of such plots, correlations between intermolecular interactions for a given property were determined.[33]

■ ASSOCIATED CONTENT

Supporting Information

Detailed considerations regarding the selection criteria for subject DAST derivatives, the most appropriate value of β_0 in the context of the subject study, as well as correlations between η_{inter} and the nonbonded contact effects. This material is available free of charge via the Internet at http://pubs.acs.org.

■ AUTHOR INFORMATION

Corresponding Authors

*Cavendish Laboratory, University of Cambridge, J. J. Thomson Avenue, Cambridge, CB3 0HE, U.K. E-mail: jmc61@cam.ac.uk (J. M.C.).

*Cavendish Laboratory, University of Cambridge, J. J. Thomson Avenue, Cambridge, CB3 0HE, U.K. E-mail: tzechia.lin@gmail.com (T.-C. L.).

Author Contributions

‡These authors contributed equally. O.P.K. and S.C.L. provided the crystal samples. J.M.C., A.J.E., and T.-C.L. performed the neutron diffraction experiments; T.-C.L. analyzed the data under supervision of J.M.C. and with assistance from R.O.P.; G.D. undertook the hyper-Rayleigh scattering measurements. J.M.C. and T.-C.L. interpreted the results and drafted the paper, with input from all authors. All authors have given approval to the final version of the manuscript.

Notes

The authors declare no competing financial interest.

■ ACKNOWLEDGMENTS

J.M.C. thanks the Fulbright Commission for a UK-US Fulbright Scholar Award hosted by Argonne National Laboratory where work done was supported by DOE Office of Science, Office of Basic Energy Sciences, under Contract No. DE-AC02-06CH11357. T.-C.L. acknowledges the Taiwanese Government for a Studying Abroad Scholarship. The Bragg Institute, ANSTO, Australia, is acknowledged for access to neutron scattering facilities via program proposal 1236. K.C. and G.D. acknowledge funding from the University of Leuven (GOA/11/003) and the Region of Flanders (FWO and Hercules). O.P.K. and S.C.L. are thankful for the support by the National Research Foundation (NRF) grants funded by the Korean Government (the Ministry of Science, ICT and Future Planning, and the Ministry of Education) (NRF-2013R1A2A2A01007232, 2014R1A5A1009799, and 2009-0093826).

■ REFERENCES

(1) Marder, S. R.; Perry, J. W.; Yakymyshyn, C. P. Organic Salts with Large Second-Order Optical Nonlinearities. *Chem. Mater.* **1994**, *6*, 1137−1147.

(2) Yang, Z.; Jazbinsek, M.; Ruiz, B.; Aravazhi, S.; Gramlich, V.; Günter, P. Molecular Engineering of Stilbazolium Derivatives for Second-Order Nonlinear Optics. *Chem. Mater.* **2007**, *19*, 3512−3518.

(3) Clays, K.; Coe, B. J. Design Strategies versus Limiting Theory for Engineering Large Second-Order Nonlinear Optical Polarizabilities in Charged Organic Molecules. *Chem. Mater.* **2003**, *15*, 642−648.

(4) Marder, S. R.; Perry, J. W.; Schaefer, W. P. Synthesis Of Organic Salts with Large Second-Order Optical Nonlinearities. *Science* **1989**, *245*, 626−628.

(5) Jazbinsek, M.; Mutter, L.; Günter, P. Photonic Applications with the Organic Nonlinear Optical Crystal DAST. *IEEE J. Sel. Top. Quantum Electron.* **2008**, *14*, 1298−1311.

(6) Cole, J. M. Organic Materials for Second-Harmonic Generation: Advances in Relating Structure to Function. *Philos. Trans. R. Soc. London A* **2003**, *361*, 2751−2770.

(7) Teshome, A.; Bhuiyan, M. D. H.; Gainsford, G. J.; Ashraf, M.; Asselberghs, I.; Williams, G. V.M; Kay, A. J.; Clays, K. Synthesis, Linear and Quadratic Nonlinear Optical Properties of Ionic Indoline and *N*,*N*-Dimethylaniline Based Chromophores. *Opt. Mater. (Amsterdam, Neth.)* **2011**, *33*, 336−345.

(8) Meier, U.; Bösch, M.; Bosshard, C.; Pan, F.; Günter, P. Parametric Interactions in the Organic Salt 4-N,N-Dimethylamino-4′-N′-Methyl-Stilbazolium Tosylate at Telecommunication Wavelengths. *J. Appl. Phys. (Melville, NY, U. S.)* **1998**, *83*, 3486−3489.

(9) Chemla, D. S.; Oudar, J. L.; Jerphagnon, J. Origin of the Second-Order Optical Susceptibilities of Crystalline Substituted Benzene. *Phys. Rev. B: Condens. Matter Mater. Phys.* **1975**, *12*, 4534−4546.

(10) Kwon, O.-P.; Kwon, S.-J.; Jazbinsek, M.; Seo, J.-Y.; Kim, J.-T.; Seo, J.-I.; Lee, Y. S.; Yun, H.; Günter, P. Phenolic Polyene Crystals with Tailored Physical Properties and Very Large Nonlinear Optical Response. *Chem. Mater.* **2011**, *23*, 239−246.

(11) Cole, J. M.; Howard, J. A. K.; McIntyre, G. J. Influence Of Hydrogen Bonding on the Second Harmonic Generation Effect: Neutron Diffraction Study of 4-Nitro-4′-Methylbenzylidene Aniline. *Acta Crystallogr., Sect. B: Struct. Sci.* **2001**, *57*, 410−414.

(12) Thalladi, V. R.; Boese, R.; Brasselet, S.; Ledoux, I.; Zyss, J.; Jetti, R. K. R.; Desiraju, G. R. Steering Non-Centrosymmetry into the Third Dimension: Crystal Engineering of An Octupolar Nonlinear Optical Crystal. *Chem. Commun. (Cambridge, U. K.)* **1999**, 1639−1640.

(13) Cole, J. M.; Goeta, A. E.; Howard, J. A. K.; McIntyre, G. J. X-Ray and Neutron Diffraction Studies of the Non-Linear Optical Compounds MBANP and MBADNP at 20 K: Charge-Density and Hydrogen-Bonding Analyses. *Acta Crystallogr., Sect. B: Struct. Sci.* **2002**, *58*, 690−700.

(14) Lin, T. C.; Cole, J. M.; Higginbotham, A. P.; Edwards, A. J.; Piltz, R. O.; Pérez-Moreno, J.; Seo, J.-Y.; Lee, S.-C.; Clays, K.; Kwon, O.-P. Molecular Origins of the High-Performance Nonlinear Optical Susceptibility in a Phenolic Polyene Chromophore: Electron Density

DOI: 10.1021/am508213c
ACS Appl. Mater. Interfaces 2015, 7, 4693−4698

Distributions, Hydrogen Bonding, and *Ab Initio* Calculations. *J. Phys. Chem. C* **2013**, *117*, 9416−9430.
(15) Kim, P.-J.; Jeong, J.-H.; Jazbinsek, M.; Kwon, S.-J.; Yun, H.; Kim, J.-T.; Lee, Y. S.; Baek, I.-H.; Rotermund, F.; Günter, P.; Kwon, O.-P. Acentric Nonlinear Optical *N*-Benzyl Stilbazolium Crystals with High Environmental Stability and Enhanced Molecular Nonlinearity in Solid State. *CrystEngComm* **2011**, *13*, 444−451.
(16) Coe, B. J.; Harris, J. A.; Asselberghs, I.; Clays, K.; Olbrechts, G.; Persoons, A.; Hupp, J. T.; Johnson, R. C.; Coles, S. J.; Hursthouse, M. B.; Nakatani, K. Quadratic Nonlinear Optical Properties of *N*-Aryl Stilbazolium Dyes. *Adv. Funct. Mater.* **2002**, *12*, 110−116.
(17) Yang, Z.; Aravazhi, S.; Schneider, A.; Seiler, P.; Jazbinsek, M.; Günter, P. Synthesis and Crystal Growth of Stilbazolium Derivatives for Second-Order Nonlinear Optics. *Adv. Funct. Mater.* **2005**, *15*, 1072−1076.
(18) Yang, Z.; Wörle, M.; Mutter, L.; Jazbinsek, M.; Günter, P. Synthesis, Crystal Structure, and Second-Order Nonlinear Optical Properties of New Stilbazolium Salts. *Cryst. Growth Des.* **2007**, *7*, 83−86.
(19) Clays, K.; Persoons, A. Hyper-Rayleigh Scattering in Solution. *Phys. Rev. Lett.* **1991**, *66*, 2980−2983.
(20) McKinnon, J. J.; Jayatilaka, D.; Spackman, M. A. Towards Quantitative Analysis of Intermolecular Interactions with Hirshfeld Surfaces. *Chem. Commun. (Cambridge, U. K.)* **2007**, 3814−3816.
(21) Spackman, M. A.; McKinnon, J. J. Fingerprinting Intermolecular Interactions in Molecular Crystals. *CrystEngComm.* **2002**, *4*, 378−392.
(22) Seidler, T.; Stadnicka, K.; Champagne, B. Second-Order Nonlinear Optical Susceptibilities and Refractive Indices of Organic Crystals from a Multiscale Numerical Simulation Approach. *Adv. Opt. Mater.* **2014**, *2*, 1000−1006.
(23) Seidler, T.; Stadnicka, K.; Champagne, B. Linear and Second-Order Nonlinear Optical Properties of Ionic Organic Crystals. *J. Chem. Phys.* **2014**, *141*, 104109/1−104109/10.
(24) Aouani, H.; Rahmani, M.; Navarro-Cia, M.; Maier, S. A. Third-Harmonic-Upconversion Enhancement from a Single Semiconductor Nanoparticle Coupled to a Plasmonic Antenna. *Nat. Nanotechnol.* **2014**, *9*, 290−294.
(25) Deng, H. D.; Li, G. C.; Dai, Q. F.; Ouyang, M.; Lan, S.; Trofimov, V. A.; Lysak, T. M. Size Dependent Competition between Second Harmonic Generation and Two-Photon Luminescence Observed in Gold Nanoparticles. *Nanotechnology* **2013**, *24*, 075201.
(26) Olbrechts, G.; Strobbe, R.; Clays, K.; Persoons, A. High-Frequency Demodulation of Multi-Photon Fluorescence in Hyper-Rayleigh Scattering. *Rev. Sci. Instrum.* **1998**, *69*, 2233−2241.
(27) Oudar, J. L.; Chemla, D. S. Hyperpolarizabilities of the Nitroanilines and Their Relations to the Excited State Dipole Moment. *J. Chem. Phys.* **1977**, *66*, 2664−2668.
(28) Levine, B. F.; Bethea, C. G. Charge Transfer Complexes and Hyperpolarizabilities. *J. Chem. Phys.* **1977**, *66*, 1070−1074.
(29) Lalama, S.; Garito, A. Origin of the Nonlinear Second-Order Optical Susceptibilities of Organic Systems. *Phys. Rev. A: At., Mol., Opt. Phys.* **1979**, *20*, 1179−1194.
(30) Edwards, A. J. Neutron Diffraction − Recent Applications to Chemical Structure Determination. *Aust. J. Chem.* **2011**, *64*, 869−872.
(31) Piltz, R. O. Accurate Data Analysis for the Koala and VIVALDI Neutron Laue Diffractometers. *Acta Crystallogr., Sect. A: Found. Crystallogr.* **2011**, *67*, C155.
(32) Sheldrick, G. M. A Short History of *SHELX*. *Acta Crystallogr., Sect. A: Found. Crystallogr.* **2008**, *64*, 112−122.
(33) McKinnon, J. J.; Spackman, M. A.; Mitchell, A. S. Novel Tools for Visualizing and Exploring Intermolecular Interactions in Molecular Crystals. *Acta Crystallogr., Sect. B: Struct. Sci.* **2004**, *60*, 627−668.

DOI: 10.1021/am508213c
ACS Appl. Mater. Interfaces 2015, 7, 4693−4698